

# Principal Modes in Graded-Index Multimode Fiber in Presence of Spatial- and Polarization-Mode Coupling

Mahdieh B. Shemirani, Wei Mao, Rahul Alex Panicker, and Joseph M. Kahn, *Fellow, IEEE*

**Abstract**—Power-coupling models are inherently unable to describe certain mode coupling effects in multimode fiber (MMF) when using coherent sources at high bit rates, such as polarization dependence of the impulse response. We develop a field-coupling model for propagation in graded-index MMF, analogous to the principal-states model for polarization-mode dispersion in single-mode fiber. Our model allows computation of the fiber impulse response, given a launched electric-field profile and polarization. In order to model both spatial- and polarization-mode coupling, we divide a MMF into numerous short sections, each having random curvature and random angular orientation. The model can be described using only a few parameters, including fiber length, number of sections, and curvature variance. For each random realization of a MMF, we compute a propagation matrix, the principal modes (PMs), and corresponding group delays (GDs). When the curvature variance and fiber length are small (low-coupling regime), the GDs are close to their uncoupled values, and scale linearly with fiber length, while the PMs remain highly polarized. In this regime, our model reproduces the polarization dependence of the impulse response that is observed in silica MMF. When the curvature variance and fiber length are sufficiently large (high-coupling regime), the GD spread is reduced, and the GDs scale with the square root of the fiber length, while the PMs become depolarized. In this regime, our model is consistent with the reduced GD spread observed in plastic MMF.

**Index Terms**—Bends, coherence bandwidth, group delays, high coupling regime, impulse response, low coupling regime, multimode fiber, polarization coupling, principal modes, spatial coupling.

## I. INTRODUCTION

**I**N A MULTIMODE fiber (MMF), different modes generally propagate with different group delays (GDs), a phenomenon known as modal dispersion. Fiber imperfections, such as index inhomogeneity, core ellipticity and eccentricity, and bends, introduce coupling between modes, an effect known as mode coupling. Because of mode coupling, even if a light pulse is launched into a single mode, it tends to couple to other modes, leading to a superposition of several pulses at the output of the MMF.

Manuscript received May 20, 2008; revised August 06, 2008. Current version published May 06, 2009. This work was supported in part by a National Science Foundation Grant EECs-0700899 and in part by a Stanford Graduate Fellowship.

M. B. Shemirani and J. M. Kahn are with the Department of Electrical Engineering, Stanford University, Stanford, CA 94305 USA (e-mail: mahdieh@stanford.edu; jmk@ee.stanford.edu).

W. Mao is with Robert Bosch LLC, Palo Alto, CA 94304 USA (e-mail: Wei.Mao@us.bosch.com).

R. A. Panicker is with Embrace, Stanford, CA 94305 USA (e-mail: rahulap@stanfordalumni.org).

Digital Object Identifier 10.1109/JLT.2008.2005066

Traditionally, modal dispersion and coupling in MMF have been described using power-coupling models [1]–[5]. Such models implicitly assume that the ideal modes and their GDs are not modified by mode coupling. Coupling simply causes a redistribution of power among the modes, and can be described by coupling coefficients that are real, non-negative and independent of phase. Such models are effective in describing the modal power distribution as a function of time and fiber length [2], and also provide a good understanding of signal distortion, pulse broadening as a function of fiber length [4], and fiber loss. Such models fail to consider phase effects, however, making them generally appropriate only for incoherent sources, such as light-emitting diodes. By contrast, in single-mode fiber (SMF), polarization-mode coupling and polarization-mode dispersion (PMD) have been described by a field-coupling model called the principal states model [6]–[9]. In this model, coupling between polarization-mode field amplitudes is described by complex coefficients that are phase-dependent. This coupling modifies the ideal modes and their GDs, making them frequency-dependent. There exists a pair of orthogonal polarization states called principal states of polarization, which are eigenmodes of the GD operator, and which have field amplitudes and GDs that are independent of frequency to first order.

In recent years, experiments have been performed in MMF using coherent sources and very high-speed modulation, exhibiting certain effects that cannot be explained using power coupling models, such as a dependence of the impulse response on the launched polarization [10]–[13]. Fan and Kahn [14] introduced a field coupling model that is a straightforward generalization of the principal states model used for SMF with PMD. In particular, their model predicts a set of orthogonal modes called principal modes (PMs), which are eigenmodes of the GD operator, and which have amplitudes and GDs that are independent of frequency to first order. In other words, the PMs are free of modal dispersion to first order in frequency. Shen *et al.* [11] used adaptive optics to launch into low-order PMs, reducing modal dispersion and enabling transmission at high bit rate-distance products, even in fibers exhibiting mode coupling. The results in [11] cannot be explained fully using power coupling models.

Reference [14] described the concept of PMs in a general, abstract setting, and did not propose any specific models for mode coupling that might be used to quantitatively explain experimental results. Hence, in this paper, we propose a parameterized physical model for graded-index MMF that allows us to compute spatial- and polarization-mode coupling coefficients, and thus to compute PMs and their delays. In the model, bending of the fiber is used to induce spatial-mode coupling and birefringence. Concatenated multiple sections

with differently oriented bends induce polarization-mode coupling.<sup>1</sup> Because spatial-mode coupling is phase dependent, and birefringence leads to different phase shifts for different launched polarizations, the model naturally leads to polarization-dependent spatial-mode coupling. The model exhibits two limiting regimes. In the low-coupling regime, the GDs are weakly dependent on mode coupling, and the differential group delays (DGDs) are linearly proportional to fiber length. By contrast, in the high-coupling regime, the GDs are strongly dependent on mode coupling. DGDs are reduced as compared to the low-coupling regime, and are proportional to the square root of fiber length.

The remainder of this paper is organized as follows. In Section II, we describe the multi-section model for a fiber with spatial- and polarization-mode coupling. Using the model, we compute the propagation operator of a fiber. We then compute the group delay operator and find its eigenvectors, which are the PMs. We also compute the impulse response of a fiber for a given launched field distribution and polarization. We provide a proof, valid in the low-coupling regime, of the orthogonality of the polarizations leading to minimum and maximum eye openings. In Section III, we study a simple three-mode system to illustrate some of the dependencies of the GDs on fiber curvature and length in the low- and high-coupling regimes. In Section IV, we describe numerical calculations of the model for realistic fibers, describing the properties of the PMs and their group delays in the low- and high-coupling regimes. We present conclusions in Section V.

## II. THEORY

We model the fiber as a concatenation of many curved sections, as shown in Fig. 1. Each section lies in a plane, with the plane of one section rotated with respect to the previous section. The curvature in each section leads to both spatial-mode coupling and birefringence. The concatenation of many curved sections leads to polarization-dependent spatial-mode coupling. This model may be viewed as an extension of the multi-section model for PMD in SMF [15]. In our model, we do not assume any mechanism for mode-dependent loss.

A complete description of modal propagation in such a fiber is provided by the propagation matrix for the entire fiber,  $\mathbf{U}_{\text{total}}$ . In deriving an expression for  $\mathbf{U}_{\text{total}}$ , we work with local normal modes [16]. Thus, in each section of the fiber, we work in the basis of the ideal modes of an unperturbed fiber, with coordinate axes aligned along the plane of that particular section. Propagation in the  $i$ th section is affected by spatial-, but not by polarization-mode coupling, and is represented by a propagation matrix,  $\mathbf{U}_{\text{prop}}^i$ . At the junction between sections  $i$  and  $i+1$ , the local axes are rotated by an angle  $\theta_i$ . Two effects must be considered here. A polarization-mode rotation matrix  $\mathbf{R}^i$  accounts for the polarization coupling due to axis rotation. Moreover, the spatial mode patterns that were defined along the previous axes must be expanded along the new axes to account for a new ideal mode basis. This is described by a spatial-mode projection matrix  $\mathbf{M}^i$ .

<sup>1</sup>Apart from modal projection along the rotated axes, spatial mode coupling also occurs at each junction between curved sections, but it is neglected in our lowest order perturbation analysis.

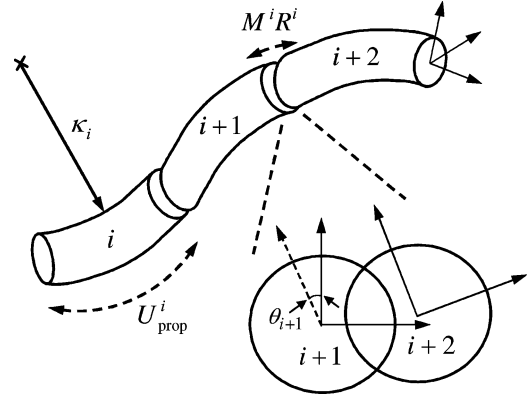


Fig. 1. Multimode fiber modeling. The fiber is divided into sections, each with random curvature and random orientation with respect to the previous section.

It is easy to show that  $[\mathbf{M}^i, \mathbf{R}^i] = 0$ , which means that the order in which the two matrices are applied does not matter. Thus

$$\mathbf{U}_{\text{total}} = \prod_{i=1}^N \mathbf{M}^i \mathbf{R}^i \mathbf{U}_{\text{prop}}^i \quad (1)$$

where  $N$  is the total number of sections.

In what follows, we describe details of our model to enable computation of each of these matrices. We first describe the refractive index profile of the fiber. We then derive propagation constants and field profiles of local normal modes, and compute spatial-mode coupling coefficients in a curved section. We combine these to obtain the  $\mathbf{U}_{\text{prop}}^i$ , and then combine these with the  $\mathbf{R}^i$  and  $\mathbf{M}^i$  to obtain  $\mathbf{U}_{\text{total}}$ . We then compute the GD operator, and obtain electric field profiles and GDs of the PMs of the fiber.

### A. Refractive-Index Profile

We use the infinite parabolic-index core approximation [5], [17], corresponding to a refractive index of the form

$$n^2 = n_{0(x,y)}^2 - 2\Delta \cdot n_0^2 \left(\frac{r}{a}\right)^\alpha \quad (2)$$

where  $n_0$  is the nominal refractive index of the center of the fiber.  $n_{0x}$  and  $n_{0y}$  are the background refractive indexes at the center of the fiber for  $x$  and  $y$  polarizations, and each differs from  $n_0$  by half of the birefringence.  $\Delta$  parameterizes the index difference between core and cladding,  $r$  is the radial distance from the center of the fiber,  $a$  is the core radius, and  $\alpha \approx 2$  is the power-law exponent. We assume that the background indices,  $n_{0x}$  and  $n_{0y}$ , depend on stress due to birefringence, while  $\Delta$  and  $n_0$  are independent of stress. In order to account for material dispersion,  $n_0$  is computed using the Sellmeier equation [18].

Birefringence, defined as the difference between refractive indexes seen at the center of the fiber by  $x$ - and  $y$ -polarized waves, is assumed to be induced by stress due to curvature [19]

$$n_{0x} - n_{0y} = \delta \frac{C_s}{2k_0} (a\kappa)^2 \quad (3)$$

where  $\kappa$  is the curvature of a fiber section, and  $C_s/k_0$  is referred to as the strain-optical coefficient. For an SMF  $C_s/k_0 = 0.0878n_0^3$  and  $\delta = 1$  [20]. In MMF, index inhomogeneity, core

ellipticity and eccentricity, bends, twists, and internal and external stresses may induce spatial-mode coupling and birefringence, although the two effects may not necessarily have identical origins in a given fiber. For simplicity, our model employs curvature to generate both effects. In order for curvature to generate physically realistic values of both effects, we must choose  $\delta \gg 1$ .

### B. Ideal Modes

Using the weak-guidance approximation, which holds when  $\Delta \ll 1$ , a closed-form solution for the ideal modes of the MMF can be obtained in both Cartesian [17] and cylindrical coordinates [21]. Due to symmetries enforced by the bends in  $x$  and  $y$  directions, it is easiest to find the coupling coefficients in Cartesian coordinates, using the eigenmodes of the ideal fiber, which are orthonormal Hermite–Gaussian functions<sup>2</sup>

$$|E_{pq}\rangle = \frac{\sqrt{\frac{2}{\pi}}}{w\sqrt{2^{p+q}p!q!}} H_p\left(\sqrt{2}\frac{x}{w}\right) H_q\left(\sqrt{2}\frac{y}{w}\right) \times e^{-\frac{x^2+y^2}{w^2}} e^{-j\beta_{pq}z}$$

$$\langle E_{pq}|E_{p'q'}\rangle = \delta_{pp'}\delta_{qq'} \quad (4)$$

where  $p$  and  $q$  are mode numbers in the  $x$  and  $y$  directions. The maximum values of  $p$  and  $q$  are determined by [5]

$$(p+q)_{\max} = p_{\max} = q_{\max} = \frac{a^2}{w^2} \quad (5)$$

and the mode radius  $w$  (different from frequency  $\omega$ ) is given by

$$w^2 = \frac{\sqrt{2}a}{k_0 n_0 \sqrt{\Delta}}. \quad (6)$$

The total number of modes is given by

$$2M = 2 \times \frac{[(p+q)_{\max} + 1][(p+q)_{\max} + 2]}{2} \quad (6)$$

where the factor 2 describes the two polarization states for each ideal spatial mode. We may, therefore, represent a spatial mode pattern at each point  $z$  along the fiber axis by a  $2M \times 1$  complex vector  $A(z)$ , in the basis of ideal modes

$$A_{(x,y)}(z) = [a_{i_1}^x(z) \cdots a_{i_M}^x(z) \ a_{i_1}^y(z) \cdots a_{i_M}^y(z)]^T \quad (8)$$

where  $i_m$  is a mode index representing  $(p, q)$ .<sup>3</sup> For the case where  $\alpha = 2$ , the propagation constant  $\beta_{pq(x,y)}$  is given by [17]

$$\beta_{pq(x,y)} = \left\{ n_0^2(x,y) k_0^2 - \frac{k_0}{a} n_0 \sqrt{2\Delta} [(2p+1) + (2q+1)] \right\}^{1/2}. \quad (9)$$

In typical fibers,  $\alpha$  differs slightly from 2 (for example, the data in [11] suggest a value of  $\alpha$  slightly greater than 2), making

<sup>2</sup>We use Heisenberg notation for electric fields.  $\langle E_{pq}|E_{p'q'}\rangle$  can denote either the vector dot product between ideal modes, or the corresponding overlap integral between the electric fields over the infinite fiber cross section  $\langle E_{pq}|E_{p'q'}\rangle = \int_{-\infty}^{\infty} \int_{-\infty}^{\infty} E_{pq}(x,y) E_{p'q'}(x,y) dx dy$ .

<sup>3</sup>In order to express the ideal mode coefficients in a single vector,  $(p, q)$  are sorted as follows:  $[(0, 0), (0, 1), \dots, (0, q_{\max}), (1, 0), \dots, (1, q_{\max} - 1), \dots, (p_{\max}, 0)]$ .

it difficult to find a closed-form solution for the ideal mode patterns. In our first-order perturbation analysis, we assume that as  $\alpha$  deviates from 2, the ideal mode patterns do not change, and only the propagation constants change. This is a standard assumption for perturbation analysis of wave equations, e.g., in quantum mechanics [22]. The propagation constants are computed for  $\alpha > 2$  in [23], but without taking birefringence into account. We have modified the expressions in [23] by assuming that the background index depends on polarization while the radially varying index does not, obtaining the propagation constants

$$\beta_{pq(x,y)} = \frac{1}{a} \left\{ (k_0 a n_0(x,y))^2 - \tilde{B}^2 \right\}^{1/2}$$

$$\tilde{B} = \left\{ \frac{\Gamma\left(\frac{1}{\alpha} + \frac{1}{2}\right) (\alpha+2)(p+q+1) \pi^{1/2} V^{2/\alpha}}{2\Gamma\left(\frac{1}{\alpha}\right)} \right\}^{\alpha/(\alpha+2)}$$

$$V = k_0 a n_0 \sqrt{2\Delta}. \quad (10)$$

We note that the propagation constants are sensitive to birefringence through  $n_0(x,y)$ . The gamma function is defined as

$$\Gamma(z) = \int_0^{\infty} t^{z-1} e^{-t} dt. \quad (11)$$

In (10),  $\beta$  is not linearly proportional to  $\omega$ , indicating group-delay dispersion.

### C. Modal Coupling Coefficients in a Single Section

In order to evaluate the modal coupling caused by the bends, using coupled-mode theory [16], we expand the mode fields in terms of local normal modes. In this method, the wave equation is solved at each  $z$  along the fiber, where the refractive index is  $n(x, y, z)$ . Assuming that any back-scattered waves do not couple to forward-propagating waves, the mode-coupling equation is

$$\frac{da_{pq}}{dz} = -j a_{pq} \beta_{pq} + \sum_{p',q'} C_{pq,p'q'} a_{p'q'} \quad (12)$$

where  $a_{pq}$  is the amplitude of wave in mode  $(p, q)$  with normalized field pattern given by (3).  $C_{pq,p'q'}$  is the coupling coefficient derived from an overlap integral taken over fiber cross section [16]

$$C_{pq,p'q'} = \frac{k_0}{2n_0} \left\langle E_{pq} \left| \frac{\partial n^2}{\partial z} \right| E_{p'q'} \right\rangle$$

$$C_{pq,p'q'} = 0 \quad \text{for } p+p' = q+q'. \quad (13)$$

The equations in [16] have been modified for normalized mode fields. It also should be noted that modes in the same group are not coupled. Let  $x_0(z)$  and  $y_0(z)$  represent the center of the fiber at position  $z$ . A perturbation of the refractive index for  $\alpha = 2$  can be expressed as [5]

$$n^2 \approx n_0^2 - \frac{2\Delta n_0^2}{a^2} \left[ (x - x_0(z))^2 + (y - y_0(z))^2 \right]. \quad (14)$$

In our model, bends are defined to be along the  $x$  direction, so  $y_0(z) = 0$ . In order for our perturbation analysis to be valid, we should have  $2\Delta \cdot x_0(z) \cdot x/a^2 \ll 1$ . Considering (14) we can write (13) as<sup>4</sup>

$$C_{pq,p'q'} = j \frac{2k_0 n_0 \Delta}{a^2} \frac{\frac{d^2 x_0(z)}{dz^2}}{(\beta_{pq} - \beta_{p'q'})^2} \langle E_{pq} | x | E_{p'q'} \rangle. \quad (15)$$

In our model with circular bends, we can write

$$x_0(z) = \frac{1}{\kappa} (1 - \cos(\kappa z)) \approx \frac{1}{2} \kappa z^2 \quad (16)$$

where  $\kappa$  is the curvature of a section, and the approximate equality is valid when the length of each curved section is much smaller than the bend radius. Substituting the second derivative of (16) into (15), we obtain

$$C_{pq,p'q'} = j \frac{2k_0 n_0 \Delta}{a^2} \frac{\kappa}{(\beta_{pq} - \beta_{p'q'})^2} \langle E_{pq} | x | E_{p'q'} \rangle. \quad (17)$$

Equation (17) is in general valid for any field propagating inside the fiber. We define the normalized one-dimensional Hermite–Gaussian modes as

$$|E_p(x)\rangle = \sqrt{\frac{\sqrt{2/\pi}}{wp!2^p}} H_p\left(\sqrt{2}\frac{x}{w}\right) e^{-\left(\frac{x}{w}\right)^2} \quad (18)$$

and we obtain the overlap integral in (17) as

$$\langle E_p(x) | x | E_{p'}(x) \rangle = \begin{cases} \frac{w}{2} \sqrt{p'+1}, & p = p' + 1 \\ \frac{w}{2} \sqrt{p'}, & p = p' - 1 \\ 0, & \text{otherwise.} \end{cases} \quad (19)$$

In (19), we see that for Hermite–Gaussian modes, curvature induces coupling only between modes for which  $|p - p'| = 1$  and  $q - q' = 0$ . Although (17) is easy to calculate and can be used in our model, for the sake of simplicity we go one step further to approximate the propagation constant difference from (9) as

$$\beta_{pq} - \beta_{p'q'} \approx \frac{\sqrt{2\Delta}}{a} (p' + q' - p - q). \quad (20)$$

Using (20) and keeping in mind that  $|p - p'| = 1$  and  $q - q' = 0$ , (17) becomes

$$C_{pq,p'q'} = j k_0 n_0 \kappa \langle E_{pq} | x | E_{p'q'} \rangle. \quad (21)$$

The simplified expression (21) was derived in [24] by approximating a bend as the junction between two straight waveguides with a crossing angle  $\Delta\theta$  (an “abrupt bend”) and calculating the coefficients in the limit  $\Delta\theta/\Delta z \rightarrow \kappa$ . This method was originally used in [25], [26] to find the power coupling from a guided mode to radiation modes.

<sup>4</sup>A straightforward application of (13) would yield  $C_{pq,p'q'} = -(2k_0 n_0 \Delta/a^2) (dx_0(z)/dz / (\beta_{pq} - \beta_{p'q'})) \langle E_{pq} | x | E_{p'q'} \rangle$ . Reference [14, ch. 4] explains that local normal modes belong to waveguides whose coordinate axes are fixed in space. As the fiber bends along  $x$ , there is a change in direction of the  $x$  axis, so the above equation should be modified by the substitution  $x_0(z) \rightarrow -j(dx_0(z)/dz / (\beta_{pq} - \beta_{p'q'}))$ , which yields (15).

Substituting (19) into (21), we can write the mode-coupling coefficients as

$$C_{pq,p'q'} = \frac{j k_0 n_0 \kappa w}{2} \{ \sqrt{p} \delta_{p,p'+1} \delta_{q,q'} + \sqrt{p'} \delta_{p,p'-1} \delta_{q,q'} \}. \quad (22)$$

We note that the coupling coefficients (22) are defined at each point along the bend, and so they are not dependent on the length of each curved section. They depend linearly on the curvature  $\kappa$ . It is important to emphasize that since they have been computed in a scalar model, they are independent of polarization.

#### D. Modal Propagation Matrix in a Single Section

Equation (12) can be written in matrix form as

$$A'_{(x,y)}(z) = (-\mathbf{\Gamma}_{(x,y)} + \mathbf{C}) A_{(x,y)}(z) \quad (23)$$

where

$$\mathbf{\Gamma}_{(x,y)}(z) = \begin{bmatrix} \Gamma_{0(x,y)} & 0 & \cdots & 0 \\ 0 & \Gamma_{1(x,y)} & & 0 \\ \vdots & & \ddots & \vdots \\ 0 & \cdots & 0 & \Gamma_{M-1(x,y)} \end{bmatrix}$$

$$\mathbf{C}(z) = \begin{bmatrix} 0 & jC_{0,1} & \cdots & jC_{0,M-1} \\ jC_{1,0} & 0 & & jC_{1,M-1} \\ \vdots & & \ddots & \vdots \\ jC_{M-1,0} & jC_{M-1,1} & \cdots & 0 \end{bmatrix}$$

$$\Gamma_{i(x,y)} = \alpha_{i(x,y)} + j\beta_{i(x,y)}$$

$$C_{ij} = C_{ji} \quad (24)$$

Closed-form solutions to (23) for degenerate  $\mathbf{\Gamma}$ , and approximate solutions for the general case, have been found in [27]. In our case  $\mathbf{\Gamma}$  is not degenerate, but  $\mathbf{\Gamma}$  and  $\mathbf{C}$  are independent of  $z$ , so we can write

$$A(\Delta l) = \mathbf{U}_{\text{prop}} A(0) \quad (25)$$

where

$$\mathbf{U}_{\text{prop}} = \begin{bmatrix} e^{(-\mathbf{\Gamma}_x + j\mathbf{C})\Delta l} & 0 \\ 0 & e^{(-\mathbf{\Gamma}_y + j\mathbf{C})\Delta l} \end{bmatrix}. \quad (26)$$

$\mathbf{U}_{\text{prop}}$  is the propagation matrix for a single section with length  $\Delta l$ . Note that  $\mathbf{U}_{\text{prop}}$  is block diagonal, so  $x$  and  $y$  polarizations do not couple within a section.

#### E. Polarization Rotation Matrix Between Sections

At the intersection between sections  $i$  and  $i + 1$ , the fiber axis rotates by an angle  $\theta_i$ . The effect of this rotation on the electric field polarization is expressed by the unitary rotation matrix

$$\mathbf{R}^i = \begin{bmatrix} \cos(\theta_i) \mathbf{I}_{M \times M} & \sin(\theta_i) \mathbf{I}_{M \times M} \\ -\sin(\theta_i) \mathbf{I}_{M \times M} & \cos(\theta_i) \mathbf{I}_{M \times M} \end{bmatrix}. \quad (27)$$

#### F. Modal Projection Matrix Between Sections

At the intersection between sections  $i$  and  $i + 1$ , assuming that the axes  $(x', y')$  in section  $i + 1$  are rotated clockwise with

respect to the axes  $(x, y)$  in section  $i$ , we can write the mode field pattern as

$$E_{pq}(x', y') = A_{pq} H_p \left( \frac{\sqrt{2}}{w} (\cos(\theta)x' - \sin(\theta)y') \right) \times H_q \left( \frac{\sqrt{2}}{w} (\sin(\theta)x' + \cos(\theta)y') \right) \times e^{-\left(\frac{x}{w}\right)^2} e^{-j\beta_{pq}z}$$

$$A_{pq} = \frac{\sqrt{\frac{2}{\pi}}}{w\sqrt{2^{p+q}p!q!}}. \quad (28)$$

Using the following properties:

$$H_p(\cos(\theta)x' - \sin(\theta)y')$$

$$= p! \sum_{k=0}^p (-1)^{p-k} \frac{\cos(\theta)^k \sin(\theta)^{p-k} H_k(x') H_{p-k}(y')}{k!(p-k)!} \quad (29a)$$

$$H_q(\sin(\theta)x' + \cos(\theta)y')$$

$$= q! \sum_{l=0}^q \frac{\cos(\theta)^l \sin(\theta)^{q-l} H_l(y') H_{q-l}(x')}{l!(q-l)!} \quad (29b)$$

$$\int_{-\infty}^{\infty} e^{-x^2} H_\alpha(x) H_\beta(x) H_\gamma(x) dx$$

$$= \begin{cases} \sqrt{\pi} \frac{2^s \alpha! \beta! \gamma!}{(s-\alpha)!(s-\beta)!(s-\gamma)!}, & \alpha + \beta + \gamma = 2s \\ & s > \alpha, s > \beta, s > \gamma \\ 0, & \text{otherwise.} \end{cases} \quad (29c)$$

closed-form expressions for decomposition of (28) along a new set of Hermite–Gaussian modes can be found in (30) shown at the bottom of the page, where

$$k + q - l + m = 2s$$

$$p - k + l + n = 2t$$

$$s > k, s > q - l, s > m, t > p - k, t > l, t > n. \quad (31)$$

Expressing the coefficients  $\xi_{mn,pq}$  in an  $M \times M$  matrix  $\Xi$ , we note that the modal projections are the same for the two polarizations, and obtain a modal projection matrix between sections  $i$  and  $i + 1$

$$\mathbf{M}^i = \begin{bmatrix} \Xi_{M \times M}^i \mathbf{I}_{M \times M} & 0 \\ 0 & \Xi_{M \times M}^i \mathbf{I}_{M \times M} \end{bmatrix}. \quad (32)$$

## G. Total Propagation Operator

Combining the results from Sections II–D–F, we obtain

$$\mathbf{U}_{\text{total}} = \prod_{i=1}^N \mathbf{M}^i \mathbf{R}^i \mathbf{U}_{\text{prop}}^i. \quad (33)$$

## H. Group-Delay Operator and Principal Modes

PMs are defined to be independent of frequency to first order, and have well-defined GDs [14]. This means that a pulse launched in an input PM is received as a single pulse in the corresponding output PM. It is shown in [14] that from the propagation operator we can obtain the GD operator

$$\mathbf{F}(\omega) = j \mathbf{U}_{\text{total}}^H(\omega) \frac{\partial \mathbf{U}_{\text{total}}(\omega)}{\partial \omega} \quad (34)$$

and that the PMs and their corresponding GDs are, respectively, the eigenvectors and eigenvalues of  $\mathbf{F}$  [14]. Let us define the PM matrix  $\mathbf{P}$ , whose columns are the eigenvectors of  $\mathbf{F}$  sorted with respect to their delays. For a lossless fiber,  $\mathbf{U}$  is unitary, and  $\mathbf{F}$  is Hermitian. Hence, the GDs are real, and  $\mathbf{P}$  is unitary. In an ideal fiber,  $\mathbf{F}$  reduces to a diagonal matrix with elements equal to the ideal-mode GDs,  $\int_0^z (\partial \beta_{pq} / d\omega) dz$ . In a fiber with mode coupling, the eigenvector decomposition (34) generally must be computed numerically.

## I. Intensity Impulse Response

If we launch light into a fiber in a mode field pattern described by a vector  $A_{\text{in}}$  (e.g., given by amplitudes in the basis of ideal modes), we can compute the amplitudes of the light that couples into each of the PMs as

$$\mu_i = \langle A_{\text{in}} | P_i \rangle \quad \text{for } i = 1, \dots, 2M. \quad (35)$$

Equation (35) can be viewed as an overlap integral over the electric fields, or as a vector dot product in the basis of ideal modes. In the latter case, this gives us a  $2M \times 1$  vector of PM amplitudes,  $\mu$ . A pulse launched into the  $i^{\text{th}}$  PM propagates with GD  $\tau_i$ . For a lossless fiber, the intensity impulse response is a sum of impulses scaled by the powers coupled into the PMs

$$h(t) = \sum_i |\mu_i|^2 \delta(t - \tau_i). \quad (36)$$

We define the intensity impulse response operator as

$$H = \sum_i |P_i\rangle \langle P_i| \delta(t - \tau_i). \quad (37)$$

$$E_{pq}(x, y) = \sum_{m,n} \xi_{mn,pq} E_{mn}(x', y')$$

$$\xi_{mn,pq} = \sum_{k=0}^p \sum_{l=0}^q \frac{\sqrt{p!q!n!m!} (-1)^{p-k} \cos(\theta)^k \sin(\theta)^{p-k} \cos(\theta)^l \sin(\theta)^{q-l}}{(s-k)!(s-q+l)!(s-m)!(t-p+k)!(t-l)!(t-n)!}, \quad (30)$$

The intensity impulse response (36) can be written as

$$h(t) = \langle A_{\text{in}} | H | A_{\text{in}} \rangle. \quad (38)$$

In matrix format, (38) is equivalent to

$$h(t) = \sum_i A_{\text{in}}^H P_i P_i^H A_{\text{in}} \delta(t - \tau_i). \quad (39)$$

### J. Orthogonality of the Polarizations Leading to Maximum and Minimum Eye Opening

In [11], it was found experimentally that holding the launched spatial mode distribution constant, the intensity impulse response is sensitive to the launched signal polarization. Moreover, it was found that in a link using on-off keying with direct detection, the polarizations leading to maximum and minimum eye openings are approximately orthogonal. In this section, we attempt to explain the latter experimental observation.

Following [11], we define the eye opening  $G$  as the difference between the power in the first spatial mode and the total power in the rest of the spatial modes. Considering birefringence to be small so that the first two delays correspond to the lowest order spatial mode in the  $x$  and  $y$  polarizations, we can write the eye opening as

$$G = |\mu_1|^2 + |\mu_2|^2 - \sum_{i \neq 1,2} |\mu_i|^2. \quad (40)$$

As we are neglecting loss, the total power  $P_{\text{tot}} = \sum_i |\mu_i|^2$  is constant, and we can maximize  $G$  by maximizing the first two terms, described by a quadratic objective function

$$G_0(\mu) = |\mu_1|^2 + |\mu_2|^2. \quad (41)$$

We assume that light is launched in a specific spatial mode pattern  $A_{M \times 1}$  with a general elliptical polarization represented as

$$A_{\text{in}} = \begin{bmatrix} A_{M \times 1} \frac{r}{\sqrt{1+r^2}} e^{j\varphi_x} \\ A_{M \times 1} \frac{1}{\sqrt{1+r^2}} e^{j\varphi_y} \end{bmatrix}. \quad (42)$$

We write  $\mu$  as

$$\mu = \mathbf{P}^H A_{\text{in}}. \quad (43)$$

Keeping the spatial mode pattern  $A_{M \times 1}$  and the total power constant, we can adjust the polarization with three degrees of freedom,  $r$ ,  $\varphi_x$  and  $\varphi_y$ . By defining a new variable  $x$

$$x = \begin{bmatrix} \frac{r}{\sqrt{1+r^2}} e^{j\varphi_x} \\ \frac{1}{\sqrt{1+r^2}} e^{j\varphi_y} \end{bmatrix} \quad (44)$$

we can express  $\mu$  as

$$\mu = \mathbf{Q}x \quad (45)$$

where

$$\mathbf{Q} = [[P_1^H \cdots P_N^H] A_{M \times 1}, [P_{N+1}^H \cdots P_{2N}^H] A_{M \times 1}]. \quad (46)$$

We define  $\tilde{\mathbf{Q}}_{2 \times 2}$  and  $\tilde{\mu}_{2 \times 1}$ , which are obtained by keeping just the first two rows of  $\mathbf{Q}$  and  $\mu$ , respectively. We define  $\zeta$  as the ratio of the maximum and minimum powers in the first two PMs

$$\begin{aligned} \zeta &= \frac{\max\{G_0(\mu)\}}{\min\{G_0(\mu)\}} = \frac{\max\{\tilde{\mu}^H \tilde{\mu}\}}{\min\{\tilde{\mu}^H \tilde{\mu}\}} = \left( \frac{\max\|\tilde{\mathbf{Q}}x\|}{\min\|\tilde{\mathbf{Q}}x\|} \right)^2 \\ &= \left( \frac{\sigma_{\max}(\tilde{\mathbf{Q}})}{\sigma_{\min}(\tilde{\mathbf{Q}})} \right)^2. \end{aligned} \quad (47)$$

where the last term is derived using singular value decomposition (SVD)

$$\begin{aligned} \max_{x \neq 0} \frac{\|\tilde{\mathbf{Q}}x\|}{\|x\|} &= \sigma_{\max}(\tilde{\mathbf{Q}}) \\ \min_{x \neq 0} \frac{\|\tilde{\mathbf{Q}}x\|}{\|x\|} &= \sigma_{\min}(\tilde{\mathbf{Q}}). \end{aligned} \quad (48)$$

Consequently,  $\zeta$  is the square of the condition number of matrix  $\tilde{\mathbf{Q}}$ . We write the SVD of  $\tilde{\mathbf{Q}}$  as

$$\tilde{\mathbf{Q}} = \tilde{\mathbf{U}} \tilde{\Sigma} \tilde{\mathbf{V}}^H. \quad (49)$$

If we choose

$$x_{\text{maximum } G} = \tilde{\mathbf{V}} \begin{bmatrix} 1 \\ 0 \end{bmatrix} \quad (50)$$

we obtain the input polarization corresponding to the maximum singular value, leading to the maximum eye opening. Conversely,

$$x_{\text{minimum } G} = \tilde{\mathbf{V}} \begin{bmatrix} 0 \\ 1 \end{bmatrix} \quad (51)$$

gives the input polarization leading to the minimum eye opening.

Here, the objective was to optimize the sum of the powers in the first and second PMs, which is of interest when trying to excite the lowest order spatial mode, and when birefringence-induced DGDs are small compared to DGDs between different spatial modes. It is straightforward to generalize the analysis to optimize the sum of the powers launched in any set of PMs while keeping the total launched power constant. By defining  $\tilde{\mathbf{Q}}$  and  $\tilde{\mu}$  appropriately, we can demonstrate the orthogonality between the launched polarizations leading to the maximum and minimum powers in the given set of PMs.

### III. ANALYTICAL MODELING OF THREE-MODE SYSTEM

In this section, we study the dependence of the GDs on fiber curvature and length in the low- and high-coupling regimes by analyzing a simple system. In a MMF (as opposed to a SMF), the minimum number of propagating modes in each polarization is three. A bend along one direction causes two of the modes to couple to each other, leaving the third mode to propagate without any coupling. Hence, we ignore this third spatial mode. For simplicity, we assume all fiber sections lie in the  $x - z$  plane, so that polarization has no effect, and can be ignored. The result is a two-mode system that is mathematically similar

to a single-mode fiber with PMD. First, to illustrate the low-coupling regime, we study a one-section fiber with known small curvature. Then, to illustrate the high-coupling regime, we study a fiber with many sections and statistical curvature parameters.

### A. DGD in Low-Coupling Regime

Here, we compute the DGD in a single section of bent fiber using an approach similar to [7]–[9]. We define the slowly varying envelope  $A(z)$  by

$$A(z) = \exp(-\Gamma z)A(0) \quad (52)$$

where  $\Gamma$  has been defined by (24). The derivative of (52) can be written as

$$A'(z) = -\Gamma e^{(-\Gamma z)}A(z) + e^{(-\Gamma z)}A'(z). \quad (53)$$

Inserting (52) and (53) into (23) we can write

$$A'(z) = j e^{(\Gamma z)} C e^{(-\Gamma z)} A(z). \quad (54)$$

This is the coupling equation for the slowly varying envelope. We define the coupling matrix for the slowly varying envelope as

$$C = e^{(\Gamma z)} C e^{(-\Gamma z)}. \quad (55)$$

Defining  $\Delta\beta = \beta_1 - \beta_2$  as the difference between the propagation constants of the two coupled modes, we can write  $C$  as

$$C = n_0 k_0 \frac{w}{2} \kappa \begin{bmatrix} 0 & e^{j\Delta\beta z} \\ e^{-j\Delta\beta z} & 0 \end{bmatrix}. \quad (56)$$

Propagation of the envelope  $A$  is described by a unitary propagation matrix  $T$ , which is similar to the Jones matrix in a SMF

$$A(z) = T(z)A(0) \quad (57)$$

$$T(z) = \begin{bmatrix} A_1(z) & -A_2^*(z) \\ A_2(z) & A_1^*(z) \end{bmatrix}. \quad (58)$$

Using  $T$ , the propagation matrix  $U$  can be found using

$$U = e^{(-\Gamma z)} T(z). \quad (59)$$

Using (59) and the fact that  $T^H T = \mathbf{I}$ , we use (34) to write the group delay matrix  $F$  as

$$F = T^H \left( -j \frac{\partial T}{\partial \omega} z + j \frac{\partial T}{\partial \omega} T^H \right) T. \quad (60)$$

Since  $T$  is unitary, the eigenvalues of  $F$  are the eigenvalues of the matrix inside the parentheses. As we see from this derivation, for a straight fiber where  $\partial T / \partial \omega = 0$ , the eigenvalues of  $F$  are the GDs of the uncoupled modes, given by  $z(\partial\beta/\partial\omega)$ . In a short section (corresponding to the low-coupling regime), we can assume that most of the light propagates in the first mode

with  $A_1(z) \approx 1$ , and gradually couples into the second mode, allowing us to obtain

$$A_2(z) = \int_0^z j C_{12}^*(z') dz' \approx j n_0 k_0 \frac{w}{2} \kappa z e^{-j \frac{\Delta\beta z}{2}}. \quad (61)$$

Using the fact that  $|A_2(z)| \propto \sqrt{w}$ ,<sup>5</sup> and considering terms only to first order in  $z$ , we can write

$$\frac{\partial A_2}{\partial \omega} \approx \frac{A_2}{2\omega}. \quad (62)$$

Taking the derivative of  $T$  in (58) and taking (62) into account

$$\frac{\partial T}{\partial \omega} = \begin{bmatrix} 0 & -\frac{A_2^*}{2\omega} \\ \frac{A_2}{2\omega} & 0 \end{bmatrix}. \quad (63)$$

Noting that (63) is equal to  $T - I/2\omega$  and inserting this into (60), we find

$$F = T^H \left( -j \frac{\partial T}{\partial \omega} z - j \frac{T^H - I}{2\omega} \right) T. \quad (64)$$

To determine the first-order effect of a single bent section, we find the GDs by solving

$$\begin{vmatrix} \frac{\partial \beta_1}{\partial \omega} z - s & -j \frac{A_2^*}{2\omega} \\ j \frac{A_2}{2\omega} & \frac{\partial \beta_2}{\partial \omega} z - s \end{vmatrix} = 0 \quad (65)$$

where the difference between the GDs gives the DGD for a fiber of total length  $L$

$$\begin{aligned} \Delta\tau &= \sqrt{\left( \frac{\partial \Delta\beta}{\partial \omega} L \right)^2 + \left| \frac{A_2(L)}{\omega} \right|^2} \\ &= L \sqrt{\left( \frac{\partial \Delta\beta}{\partial \omega} \right)^2 + \left( \frac{n_0 k_0 w \kappa}{2\omega} \right)^2}. \end{aligned} \quad (66)$$

The expression (66) shows that the DGD grows linearly with the fiber length  $L$ , like the case of PMD in the low-coupling regime. Moreover, for small  $\kappa$ , bending adds a DGD that is proportional to  $\kappa^2$ .

### B. DGD in High-Coupling Regime

In the high-coupling regime, the GDs are not determined by local fiber properties; instead, they depend on the collective effects of mode coupling over the entire fiber [7]. The statistical properties of the GDs can be studied by solving coupled stochastic differential equations. For the case of SMF with PMD, Poole [6] has examined these equations in the low- and high-coupling regimes. For a three-mode MMF that is assumed to lie in the  $x-z$  plane, the coupled-mode equations in (23) reduce to

$$A'(z) = j \begin{bmatrix} -\beta_1 & n_0 k_0 \frac{w}{2} \kappa(z) \\ n_0 k_0 \frac{w}{2} \kappa(z) & -\beta_2 \end{bmatrix} A(z). \quad (67)$$

<sup>5</sup>From (6), we note that  $w$  is proportional to  $k_0^{-1/2}$ , which result in  $|A_2(z)|$  being proportional to  $k_0^{1/2}$  or  $\omega^{1/2}$ . Using (9), we note that in the phase of equation (61),  $\Delta\beta$  is a function of  $\omega$ , but taking the derivative of the phase results to a term of order  $z^2$ , which is neglected to first order in  $z$ . Thus, the dominant factor in the derivative is the magnitude of the envelope and not the phase.

As in the previous subsection, one mode does not couple to the other two, and so is neglected in our analysis. The autocorrelation of the fiber curvature  $\kappa(z)$ , is defined as<sup>6</sup>

$$R_\kappa(u) = \langle \kappa(z)\kappa(z-u) \rangle \quad (68)$$

where the brackets denote ensemble average. We also define the power spectral density (PSD) of  $\kappa$  as

$$S_\kappa\left(\frac{\Delta\beta}{2\pi}\right) = \int_{-\infty}^{\infty} R_\kappa(u)e^{-j\Delta\beta u} du. \quad (69)$$

Following the approach of [6] in solving the stochastic coupled (67), we find the mean-square DGD as a function of  $z$  to be

$$E[\Delta\tau^2(z)] = \left(\frac{\partial\Delta\beta}{\partial\omega}\right)^2 \left[ \frac{\exp(-2hz) - 1 + 2hz}{2h^2} \right]. \quad (70)$$

The parameter  $h$  describes the ensemble-average rate at which power is transferred between modes, and is defined as

$$h = \left(n_0 k_0 \frac{w}{2}\right)^2 S_\kappa\left(\frac{\Delta\beta}{2\pi}\right). \quad (71)$$

In the low-coupling limit  $hz \rightarrow 0$ , we have

$$\lim_{hz \rightarrow 0} E[\Delta\tau^2(z)] \Big|_{z=L} = \left(\frac{\partial\Delta\beta}{\partial\omega}\right)^2 L^2 \quad (72)$$

The mean-square DGD in (72) is consistent with the DGD (66) for a fiber with one constant bend in the low-coupling regime. Equation (66) has been extended to include the effect of bending to the lowest nonzero order.

In the high-coupling limit  $hz \rightarrow \infty$ , which is what we are considering here, we find

$$\lim_{hz \rightarrow \infty} E[\Delta\tau^2(z)] \Big|_{z=L} = \left(\frac{\partial\Delta\beta}{\partial\omega}\right)^2 \frac{L}{h}. \quad (73)$$

Equation (73) gives us insight into the dependence of the DGD on the fiber statistics. It shows that in the high-coupling regime, the DGD varies inversely with the PSD of curvature. Also as in the case of PMD in SMF [6], the DGD varies with the square root of length (i.e.,  $\sqrt{L}$ ) in the high-coupling regime.

In order to get further insight into (73), we notice that in our model, since the curvature  $\kappa(z)$  is constant over each section length, the curvature can be described by a discrete random variable  $\kappa_i$ ,  $i = 1, \dots, N$ , which is independent and identically distributed (i.i.d.). Denoting the mean and variance of  $\kappa_i$  as  $m_\kappa$  and  $\sigma_\kappa^2$ , respectively, the discrete autocorrelation between sections  $i$  and  $j$  is

$$E[\kappa_i \kappa_j] = \begin{cases} \sigma_\kappa^2 + m_\kappa^2 & i = j \\ m_\kappa^2 & i \neq j \end{cases}. \quad (74)$$

In order to find the PSD of the curvature  $\kappa(z)$ , we note that  $\kappa(z)$  (a function of  $z$ ) is analogous to a PAM signal (a function of  $t$ ),

<sup>6</sup>In order to define the autocorrelation, we have averaged the curvature  $\kappa(z)$  over the length of one section in order to convert it from a cyclostationary random process to a wide-sense-stationary random process.

whose PSD is well known [28]. Using this analogy, the PSD of  $\kappa(z)$  is found to be

$$S_\kappa\left(\frac{\Delta\beta}{2\pi}\right) = \sigma_\kappa^2 \Delta l \text{sinc}^2\left(\frac{\Delta\beta}{2\pi} \Delta l\right) + m_\kappa^2 \delta\left(\frac{\Delta\beta}{2\pi} \Delta l\right). \quad (75)$$

In the present problem, where the first and second modes are non-degenerate (i.e.  $\Delta\beta \neq 0$ ), we find the DGD variance (73) to be

$$\lim_{hz \rightarrow \infty} E[\Delta\tau^2(z)] \Big|_{z=L} = \left(\frac{\partial\Delta\beta}{\partial\omega}\right)^2 \frac{L}{(n_0 k_0 \frac{w}{2} \sigma_\kappa)^2 \Delta l \text{sinc}^2\left(\frac{\Delta\beta}{2\pi} \Delta l\right)}. \quad (76)$$

Equation (76) shows that in the high-coupling regime, the DGD is proportional to the square root of fiber length (i.e.,  $\sqrt{L}$ ), and is inversely proportional to the curvature standard deviation  $\sigma_\kappa$ .

#### IV. NUMERICAL MODELING OF MULTIMODE FIBER

Based on the model described in Section II, we have performed numerical modeling of MMF using a high-precision matrix toolbox written for MATLAB [29]. The fiber is a 50- $\mu\text{m}$ -core graded-index silica MMF of total length  $L = 1000$  m. The fiber has a numerical aperture  $\text{NA} = 0.19$ , and the wavelength is  $\lambda = 1550$  nm. The refractive index at the center of the fiber is  $n_0 = 1.444$  at  $\lambda = 1550$  nm. Away from this wavelength,  $n_0$  is computed using the Sellmeier equation [18], [20]. The frequency derivative of the index,  $dn_0/d\omega$  is also computed using the Sellmeier equation. We find that in our model, however, waveguide dispersion has a much greater effect than material dispersion. The birefringence scale factor is set to  $\delta = 8000$ .<sup>7</sup> Using (5) and (7), we find that 55 spatial modes propagate in each of two polarizations. We use the infinite-core approximation (2) with  $\alpha = 2.09$ , chosen to match experiments [11] in which the lower-order modes were found to have shorter GDs, and the DGDs were found to be higher than those predicted by the ideal value  $\alpha = 2$ . Unless noted otherwise, the fiber is divided into  $10^4$  sections, each 0.1 m long. Each section is rotated with respect to the previous one by an i.i.d. angle  $\theta$ , whose probability density function (pdf) is normal with variance  $\sigma_\theta^2 = 0.36$  rad<sup>2</sup>. The curvature of each section is an i.i.d. random variable  $\kappa_i$  whose pdf is the positive side of a normal pdf, and which has variance  $\sigma_\kappa^2$ .<sup>8</sup> As  $\sigma_\kappa^2$  is increased, the model goes from the low-coupling regime to the high-coupling regime.<sup>9</sup> Given a random realization of the rotation angles and the curvatures, we compute the group delay operator  $F$ . We diagonalize  $F$  to find the PMs and their GDs.

Fig. 2(a)–(c) shows the GDs versus the curvature standard deviation  $\sigma_\kappa$  for various choices of parameters in the model. Fig. 2(a) shows GDs for a fiber with  $N = 100$  sections, each 10

<sup>7</sup>For a typical curvature value  $\kappa = 1$  m<sup>-1</sup>, using (3), we obtain a birefringence  $n_x - n_y \approx 7 \times 10^{-7}$ , which is physically reasonable.

<sup>8</sup>As the pdf of curvature is the positive side of a normal pdf  $N(0, \sigma^2)$ , its mean and variance are given by  $m_\kappa = (2/\pi)^{1/2} \sigma$ ,  $\sigma_\kappa^2 = (1 - 2/\pi) \sigma^2$ .

<sup>9</sup>Typical silica fibers correspond to the low-coupling regime [11], while typical plastic fibers correspond to the high-coupling regime [4]. Although we use parameters corresponding to silica fibers for the sake of consistency, the case of high-coupling is intended to qualitatively represent plastic fibers.

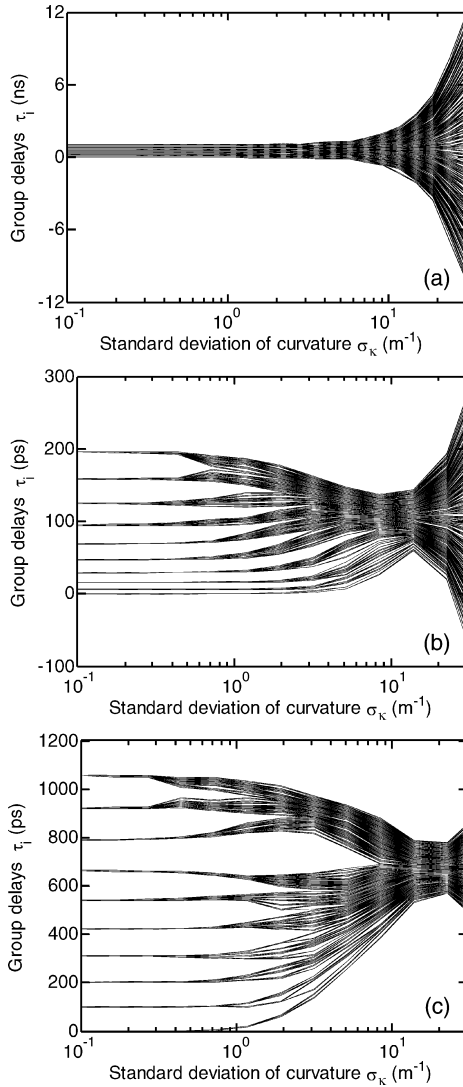


Fig. 2. Group delays versus curvature standard deviation for 1 km fiber. (a)  $\alpha = 2.09$ ,  $N = 100$  sections. (b)  $\alpha = 2.00$ ,  $N = 10^4$  sections. (c)  $\alpha = 2.09$ ,  $N = 10^4$  sections.

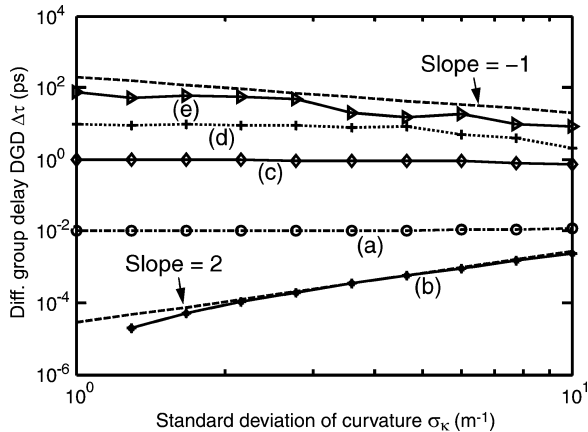


Fig. 3. Delay versus curvature standard deviation for a three-mode system. The section length is 0.1 m, while the total length  $L$  is varied. (a)  $L = 0.1$  m ( $N = 1$ ). (b)  $L = 0.1$  m ( $N = 1$ ), removing the DGD that is independent of  $\sigma_\kappa$ . (c)  $L = 10$  m ( $N = 100$ ). (d)  $L = 100$  m ( $N = 1000$ ). (e)  $L = 1000$  m ( $N = 10^4$ ).

m long. At low  $\sigma_\kappa$ , the GDs are essentially independent of  $\sigma_\kappa$ , and at very high  $\sigma_\kappa$ , the GDs diverge. Given the values chosen

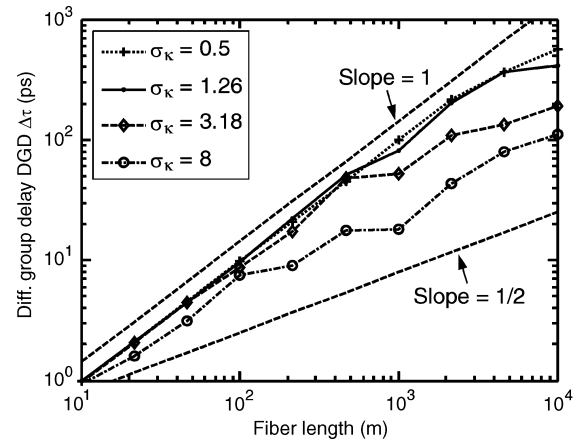


Fig. 4. Differential group delays versus fiber length in low- and high-coupling regimes.

for the various parameters in the model, this value of  $N$  is too small to generate the behavior expected from the statistical analysis in Section III-B, especially convergence of the GDs at moderate-to-high  $\sigma_\kappa$ . As we increase  $N$  to the order of  $10^4$ , the model yields results that are substantially independent of  $N$ . Fig. 2(b) and (c) considers  $N = 10^4$  sections, each 0.1 m long, for two different values of the index power-law exponent  $\alpha$ . In Fig. 2(b), where  $\alpha = 2$ , the spread between maximum and minimum GDs is just 200 ps, which is much smaller than that found experimentally [11]. Hence, in Fig. 2(c), we have increased the exponent to  $\alpha = 2.09$ , which generates realistic GD spreads. In Fig. 2(c), we can distinguish several regimes. At very small  $\sigma_\kappa$ , there is little mode coupling, and the GDs are degenerate. At slightly larger  $\sigma_\kappa$ , corresponding to low coupling, the degeneracies are broken, and the GDs are approximately quadratic in  $\sigma_\kappa$ . At high  $\sigma_\kappa$  ( $\sigma_\kappa$  between 1 and  $10 \text{ m}^{-1}$ ), corresponding to the high-coupling regime, the GDs converge, and the GD spread is reduced significantly. This behavior is qualitatively consistent with (76). Finally, at very high  $\sigma_\kappa$  (above  $20 \text{ m}^{-1}$ ), the GDs diverge. This nonphysical behavior results from a violation of the assumption made in our perturbation analysis.<sup>10</sup>

In Fig. 2(c), the convergence of GDs in the high-coupling regime is analogous to SMF with PMD, where the DGD is reduced substantially in the high-coupling regime [6]. The dependence of GDs on mode coupling is a key feature in field-coupling models, but does not occur in power-coupling models. A reduction of pulse spreading has been observed in plastic MMFs, where it was attributed to mode coupling, and was explained using a power-coupling model [4]. The reduction of pulse spreading was not attributed to changes in GDs themselves. Instead, it was argued that as a ray of light propagates, it hops from mode to mode, and all rays tend to spend nearly the same fraction of time in the respective modes, so that all rays are subject to nearly equal propagation delays. The present work provides an alternate explanation of the reduced pulse spreading in terms of changes in the GDs caused by mode coupling. We

<sup>10</sup>In order for the perturbed infinitely parabolic index profile (14) to approximate the actual graded-index profile, we must assume that  $2\Delta \cdot x(z) \cdot x_0/a^2 \ll 1$ . Using (16) and considering that light is confined in a mode of radius  $w$  near the center of the fiber, we can state this approximation as  $\Delta \cdot w \cdot \kappa \cdot \Delta l^2/a^2 \ll 1$ . In the high-coupling regime with large curvature values, this assumption can be violated if  $\Delta l$  is not sufficiently small. This is the reason for the observed divergence of the GDs.

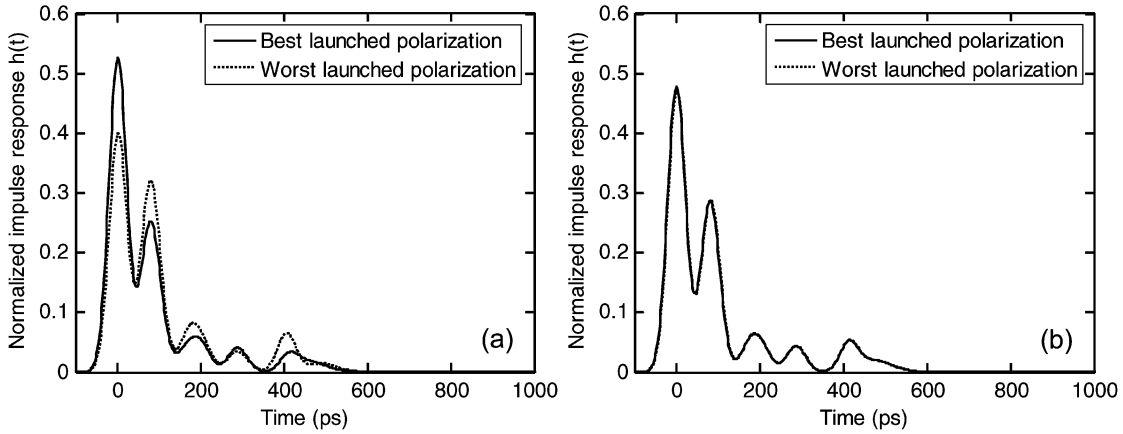


Fig. 5. Intensity impulse response for 1-km fiber with  $N = 10^4$  sections and curvature variance  $\sigma_\kappa = 1.2 \text{ m}^{-1}$ . In both cases,  $n_0(x, y)$  is taken to depend on bending-induced stress. (a)  $\Delta$  and  $n_0$  depend on stress. (b)  $\Delta$  and  $n_0$  do not depend on stress.

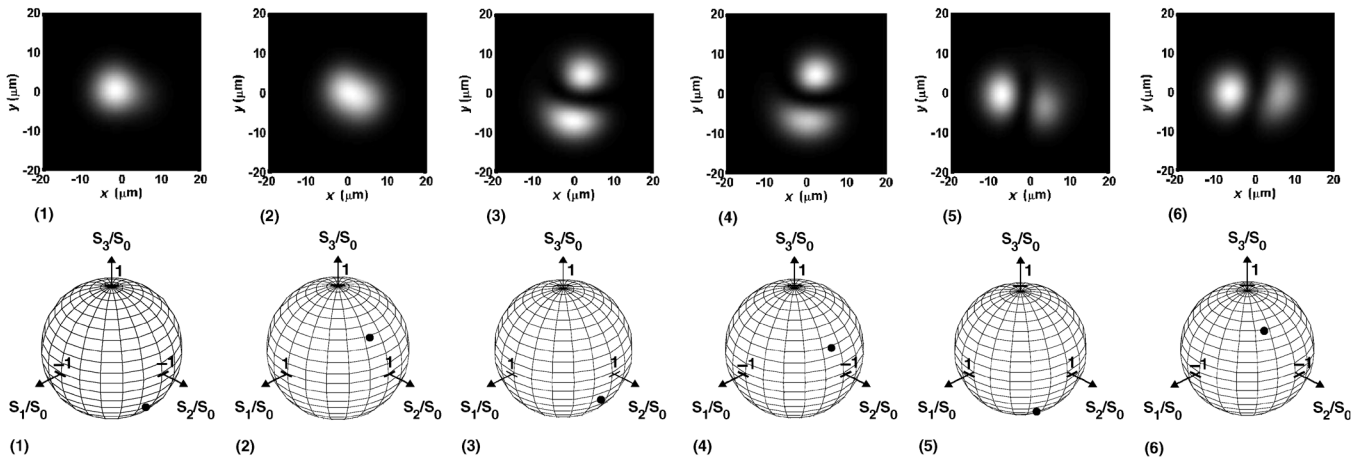


Fig. 6. Lowest order input principal modes in low-coupling regime: intensity patterns and states of polarization. The 1-km fiber has  $N = 10^4$  sections and curvature variance  $\sigma_\kappa = 0.95 \text{ m}^{-1}$ .

should note that in plastic MMF, the scattering mechanisms causing mode coupling are associated with increased attenuation. By contrast, in our model, the curvature causing mode coupling does not lead to attenuation.

In order to study the dependence of GDs on curvature standard deviation  $\sigma_\kappa$  and on fiber length  $L$ , we define the DGD  $\Delta\tau$  as the GD difference between the two lowest order PMs.<sup>11</sup>

In Fig. 3, we present the DGD  $\Delta\tau$  versus curvature standard deviation  $\sigma_\kappa$  for a three-mode system computed using our numerical MMF model. In the theoretical analysis of the three-mode system in Section III, for simplicity, we considered all fiber sections to lie in the  $x$ - $z$  plane. In the numerical model, we relax that assumption and include rotations between sections, yet obtain results consistent with the simplified analysis. In Fig. 3(a) and (b), we consider  $N = 1$  section, in which case,  $\sigma_\kappa$  reduces to a single curvature  $\kappa$ . In Fig. 3(a),  $\Delta\tau$  appears to be independent of  $\kappa$ , so in Fig. 3(b), we have removed the portion of  $\Delta\tau$  that is independent of  $\kappa$ , revealing a contribution that is proportional to  $\kappa^2$ , which is consistent with (66). In Fig. 3(c)–(e), we consider  $N = 100, 1000, 10^4$  sections, respectively. In the

<sup>11</sup>Our MMF model, with parameters chosen, generates PMD-induced DGDs that are small compared to GD differences between spatial modes. Hence, the GD of a given PM is defined as the average of the GDs in the two orthogonal polarizations.

latter case, we see that  $\Delta\tau$  is inversely proportional to  $\sigma_\kappa$ , which is consistent with (76).

In Fig. 4, we present the DGD  $\Delta\tau$  versus total length  $L$  for a MMF with  $2 \times 55$  modes. The section length is held constant at 0.1 m, so as we increase  $L$  from 10 to  $10^4$  m, the number of sections  $N$  varies from 100 to  $10^5$ . We consider four different values of the curvature variance  $\sigma_\kappa$ . When  $\sigma_\kappa$  and/or  $N$  are small,  $\Delta\tau$  is proportional to  $L$ , which is consistent with (66). For larger values of  $\sigma_\kappa$ , when  $N$  is sufficiently large,  $\Delta\tau$  tends toward a proportionality to  $\sqrt{L}$ , which is consistent with (73) and (76).

Once we have found the PMs and their respective GDs for a particular realization of a MMF, given a launched field distribution, we compute the intensity impulse response by using the impulse response operator defined in (38) and (39). This operator yields a series of impulses scaled by the powers launched into the various PMs, and delayed by their respective GDs. We convolve the intensity impulse responses with a Gaussian pulse having 50-ps full-width at half-maximum, in order to facilitate comparison with experimental measurements made with finite bandwidth [11].

Fig. 5(a) and (b) shows the intensity impulse response for a typical realization of a 1-km-long MMF, which is modeled using

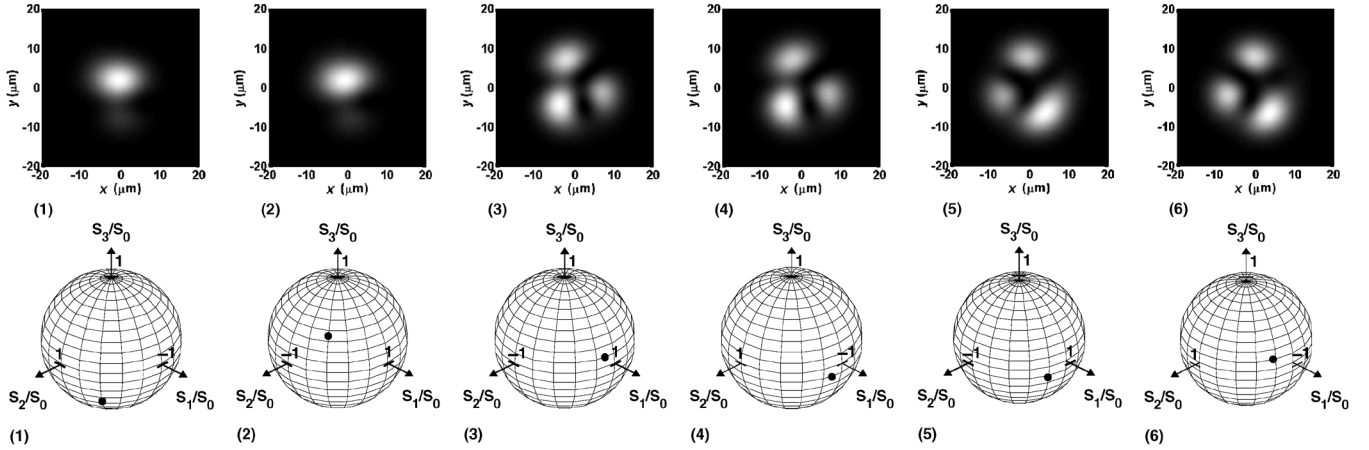


Fig. 7. Lowest order output principal modes in low-coupling regime: intensity patterns and states of polarization. The 1-km fiber has  $N = 10^4$  sections and curvature variance  $\sigma_\kappa = 0.95 \text{ m}^{-1}$ .

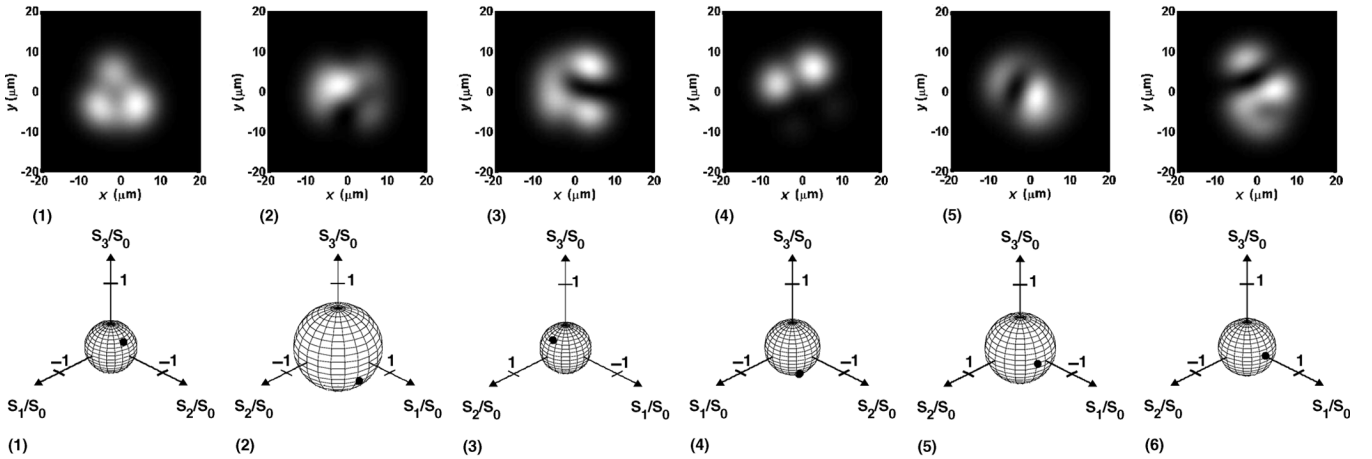


Fig. 8. Lowest order input principal modes in high-coupling regime: intensity patterns and states of polarization. The 1-km fiber has  $N = 10^4$  sections and curvature variance  $\sigma_\kappa = 4.2 \text{ m}^{-1}$ .

$N = 10^4$  sections and curvature variance  $\sigma_\kappa = 1.2 \text{ m}^{-1}$ , corresponding to low coupling. The light is launched into a Gaussian mode having radius  $w = 8 \text{ }\mu\text{m}$ , corresponding to the lowest order ideal spatial mode. These parameters are chosen to qualitatively reproduce the experimental results in [11].

In Fig. 5(a), we assume that  $n_{0(x,y)}$  depends on bending-induced stress, while  $\Delta$  and  $n_0$  are independent of stress (see the discussion of (2)). We see that as we change the launched polarization, the amount of light coupled into higher-order PMs changes substantially, in qualitative agreement with experimental observations [11], [10]. Using (50) and (51), we find the two orthogonal polarizations that lead to maximum and minimum eye openings. In the two polarizations, we observe a ratio of the maximum to minimum power in the lowest order PM to be  $\zeta = 1.31$ . To our knowledge, this work is the first explanation of the polarization dependence of the MMF impulse response.

In Fig. 5(b), we consider the same MMF realization, but assume that  $n_{0(x,y)}$ ,  $\Delta$  and  $n_0$  all depend on stress. The impulse response barely depends on polarization, and we observe  $\zeta = 1.01$ . This illustrates that the assumption that  $\Delta$  and  $n_0$  are inde-

pendent of stress is crucial in our model. Hence, this assumption is made in all calculations presented hereafter.

In Figs. 6–9, we present intensity patterns and polarization states for the lowest order input and output PMs of a 1-km fiber in the low- and high-coupling regimes. Within each figure, the PMs form pairs with nearly equal GDs, and are sorted in order of increasing GD. In order to obtain intensity patterns, we superpose the fields having different mode numbers but the same polarization, compute the intensity of each superposition, then add the intensities of the two polarizations. We present polarization states in terms of Stokes parameters [30]. In order to compute these for the  $i^{\text{th}}$  PM, we change the usual product between field components into a dot product between vectors of PM amplitudes

$$S_0 = P_{ix}^H \cdot P_{ix} + P_{iy}^H \cdot P_{iy} \quad (77a)$$

$$S_1 = P_{ix}^H \cdot P_{ix} - P_{iy}^H \cdot P_{iy} \quad (77b)$$

$$S_2 = P_{iy}^H \cdot P_{ix} + P_{ix}^H \cdot P_{iy} \quad (77c)$$

$$S_3 = j (P_{iy}^H \cdot P_{ix} - P_{ix}^H \cdot P_{iy}) \quad (77d)$$

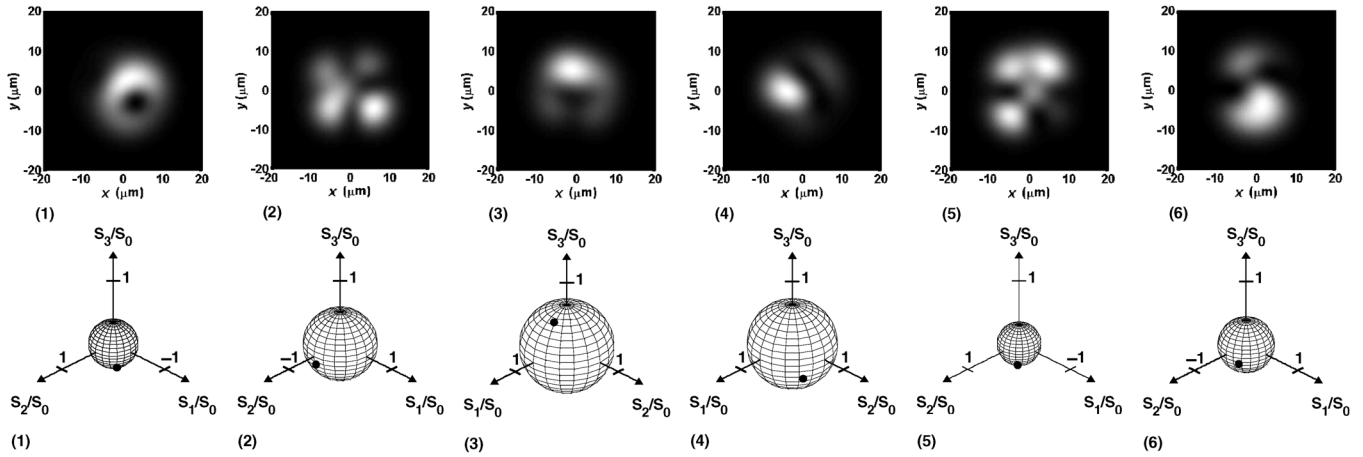


Fig. 9. Lowest order output principal modes in high-coupling regime: intensity patterns and states of polarization. The 1-km fiber has  $N = 10^4$  sections and curvature variance  $\sigma_\kappa = 4.2 \text{ m}^{-1}$ .

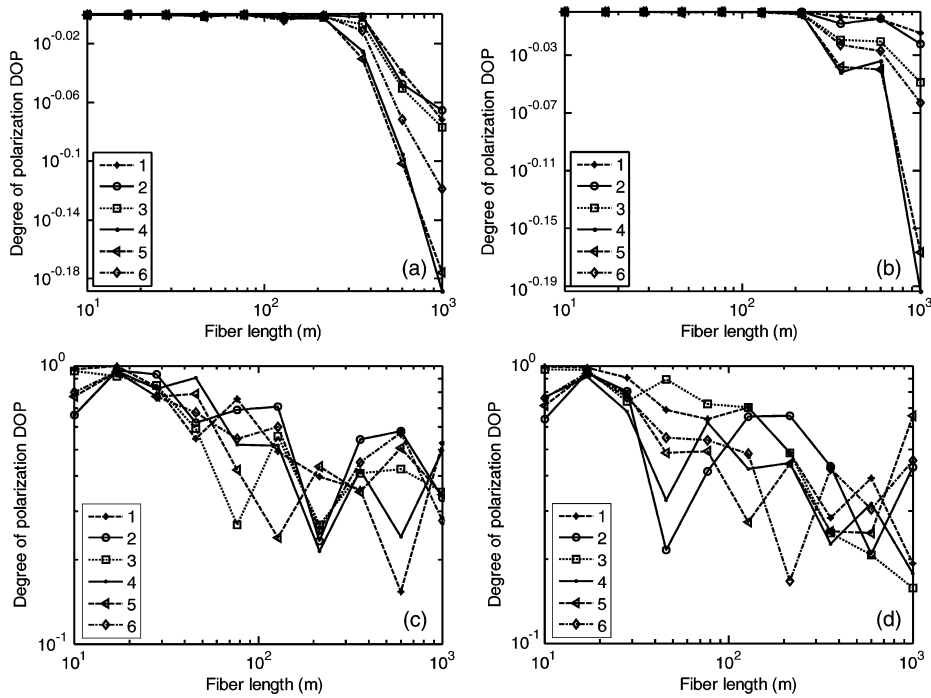


Fig. 10. Degree of polarization versus fiber length for different principal modes: (a) low-coupling regime ( $\sigma_\kappa = 0.95 \text{ m}^{-1}$ ), input principal modes; (b) low-coupling regime ( $\sigma_\kappa = 0.95 \text{ m}^{-1}$ ), output principal modes; (c) high-coupling regime ( $\sigma_\kappa = 4.2 \text{ m}^{-1}$ ), input principal modes; (d) high-coupling regime ( $\sigma_\kappa = 4.2 \text{ m}^{-1}$ ), output principal modes.

$S_1$ ,  $S_2$  and  $S_3$  are normalized to the total power  $S_0$ , and the three normalized values are shown as a point on the surface of a sphere. A radius close to 1 indicates a high degree of polarization (DOP), while a smaller radius indicates a lower DOP.

Comparing Fig. 6 to Fig. 7 and comparing Fig. 8 to Fig. 9, we observe that in all cases, an input PM and the corresponding output PM have different intensity patterns and different states of polarization.

Figs. 6 and 7 describe a 1-km MMF in the low-coupling regime, with curvature variance  $\sigma_\kappa = 0.95 \text{ m}^{-1}$ . The intensity patterns of the low-order PMs are somewhat less symmetric than those of low-order ideal modes. Within each pair of PMs having nearly identical GDs, the two have nearly identical intensity patterns but nearly orthogonal polarization states. Careful examination reveals that the very lowest order PMs 1 and 2 have DOPs

very close to 1, while PMs 3, 4, 5 and 6 exhibit DOPs slightly less than 1.

Figs. 8 and 9 describe a 1-km MMF in the high-coupling regime, with curvature variance  $\sigma_\kappa = 4.2 \text{ m}^{-1}$ . Even the lowest order PMs represent a superposition of several ideal modes, so their intensity patterns are complex and asymmetric. Within each pair of PMs having nearly identical GDs, the two have markedly different intensity patterns and polarization states. The PMs are only partially polarized, exhibiting DOPs significantly less than 1, which is indicative of significant coupling between spatial and polarization degrees of freedom.

The effects of fiber length and curvature variance on the DOP are presented in Fig. 10. The PMs are sorted by increasing GDs, with 1–2, 3–4 and 5–6 forming nearly degenerate pairs. Fig. 10(a) and (b) shows the DOP versus fiber length in the

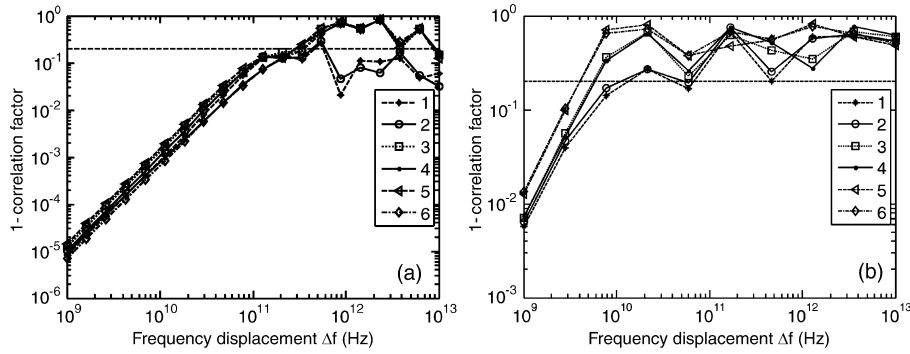


Fig. 11. Correlation factor between principal mode field patterns versus frequency displacement for a 1-km fiber in low-coupling regime ( $\sigma_\kappa = 1.2 \text{ m}^{-1}$ ): (a)  $\alpha = 2.09$ , (b)  $\alpha = 2.00$ . The horizontal line indicates a correlation factor equal to 0.8.

low-coupling regime ( $\sigma_\kappa = 0.95 \text{ m}^{-1}$ ). The PMs begin to show some depolarization at a fiber length of several hundred m, with the higher-order PMs tending to depolarize faster than the lower-order PMs as the fiber length is increased. Fig. 10(c) and (d) shows the DOP versus fiber length in the high-coupling regime ( $\sigma_\kappa = 4.2 \text{ m}^{-1}$ ). The PMs begin to show depolarization even at fiber lengths as short as 10 m, and there is no obvious, consistent correlation between mode number and DOP as the fiber length is increased.

By definition, PMs have field patterns that are independent of frequency to first order [14]. One would expect these field patterns to be approximately invariant over some frequency range, which we will refer to as a “coherence bandwidth”. In the special case of SMF with PMD, this coherence bandwidth is called the “bandwidth of the principal states of polarization” [31]. Reference [11] demonstrated the use of a spatial light modulator (SLM) to control the electric field launched into a MMF so as to preferentially excite low-order PMs, reducing the impact of modal dispersion. It was found that a single setting of the SLM could compensate for modal dispersion over a bandwidth of about 600 GHz in an 11-km silica MMF that exhibited low mode coupling. This implies that the coherence bandwidth of the PMs may be of the order of tens to hundreds of GHz in such fibers.

In order to estimate the coherence bandwidth in our model, we compute the PMs at a given optical frequency  $f = \omega/(2\pi)$  and a displaced frequency  $f + \Delta f$ , and we compute a correlation factor, which is the magnitude of the normalized inner product between the PMs at the two frequencies. We arbitrarily define the coherence bandwidth to be the value of  $\Delta f$  such that the correlation factor is reduced to 0.8. Fig. 11(a) and (b) shows the correlation factor versus frequency displacement for the lowest order PMs (numbered 1–6) in a 1-km MMF in the low-coupling regime ( $\sigma_\kappa = 1.2 \text{ m}^{-1}$ ). In Fig. 11(a), we consider an index power-law exponent  $\alpha = 2.00$  which, as shown in Fig. 2(b), gives a GD spread that is about a factor of five lower than what is observed experimentally. Using this value of  $\alpha$ , the model predicts that the PMs have coherence bandwidths of about 300 GHz. In Fig. 11(b), we consider  $\alpha = 2.09$ , which was shown in Fig. 2(c) to yield a more realistic GD spread. Using this value of  $\alpha$ , the model predicts that the lowest order PMs (1–2) have coherence bandwidths close to 10 GHz, while higher-order PMs (3–4 and 5–6) have progressively smaller coherence bandwidths. Thus, our model estimates coherence bandwidths that

are at least an order of magnitude smaller than expected from experiment. At present, the source of this discrepancy is not clear.

## V. CONCLUSIONS

We have described a field-coupling model for propagation in graded-index MMF, which is analogous to the principal-states model for PMD in SMF. Our model allows computation of the fiber impulse response, given a launched electric-field profile and polarization. In order to model both spatial- and polarization-mode coupling, we divide a MMF into a number of short sections, each having random curvature and random angular orientation. The model can be described using only a few parameters, including fiber length, number of sections, and curvature variance. For each random realization, we compute a propagation matrix, from which we obtain the PMs and their corresponding GDs. When the curvature variance and fiber length are small (low-coupling regime), the GDs are close to their uncoupled values, and scale linearly with fiber length, while the PMs remain highly polarized. In this regime, we have reproduced the polarization dependence of the impulse response that is observed in silica MMF. We have estimated the coherence bandwidths of the PMs in the low-coupling regime, obtaining estimates that are about an order of magnitude smaller than experimentally observed values. When the curvature variance and fiber length are sufficiently large (high-coupling regime), the GD spread is reduced, and the GDs scale with the square root of fiber length, while the PMs become depolarized. In this regime, our model is consistent with the reduced GD spread observed in plastic MMF.

## REFERENCES

- [1] R. Olshansky, “Mode coupling effects in graded-index optical fibers,” *Appl. Opt.*, vol. 14, no. 4, pp. 935–945, Apr. 1975.
- [2] K.-I. Kitayama, S. Sikai, and N. Uchida, “Impulse response prediction based on experimental Mode coupling coefficient in a 10-km long graded-index fiber,” *IEEE J. Quantum Electron.*, vol. QE-16, no. 3, pp. 356–362, Mar. 1980.
- [3] D. Gloge, “Optical power flow in multimode fibers,” *Bell Syst. Tech. J.*, vol. 51, no. 8, pp. 1767–1780, Oct. 1972.
- [4] A. F. Garito, J. Wang, and R. Gao, “Effects of random perturbations in plastic optical fibers,” *Science*, vol. 281, pp. 962–967, Aug. 1998.
- [5] D. Marcuse, “Losses and impulse response of a parabolic index fiber with random bends,” *Bell Syst. Tech. J.*, vol. 52, no. 8, pp. 1423–1437, Oct. 1973.

- [6] C. D. Poole, "Statistical treatment of polarization dispersion in single-mode fiber," *Opt. Lett.*, vol. 13, no. 8, pp. 687–689, Aug. 1988.
- [7] C. D. Poole and R. E. Wagner, "Phenomenological approach to polarization dispersion in long single-mode fibers," *Electron. Lett.*, vol. 22, no. 19, pp. 1029–1030, Sep. 1986.
- [8] D. A. Nolan and M. J. Li, "Fiber spin-profile designs for producing fibers with low polarization mode dispersion," *Opt. Lett.*, vol. 23, no. 21, pp. 1659–1661, Nov. 1998.
- [9] D. A. Nolan, X. Chen, and M. J. Li, "Fibers with low polarization-mode dispersion," *J. Lightw. Technol.*, vol. 22, no. 4, pp. 1066–1076, Apr. 2004.
- [10] S. Bottacchi, *Multi-Gigabit Transmission Over Multimode Optical Fiber*. New York: Wiley, 2006, pp. 594–628.
- [11] X. Shen, J. M. Kahn, and M. A. Horowitz, "Compensation for multimode fiber dispersion by adaptive optics," *Opt. Lett.*, vol. 30, no. 22, pp. 2985–2987, Nov. 2005.
- [12] S. H. Yam, F. T. An, M. E. Marhic, and L. G. Kazovsky, "Polarization sensitivity of 40 Gb/s transmission over short reach 62.5  $\mu\text{m}$  multimode fiber using single-mode transceivers," in *Proc. Opt. Fiber Commun. Conf.*, Los Angeles, CA, Feb. 23–27, 2004, vol. 2, p. 3.
- [13] E. Rochat, S. D. Walker, and M. C. Parker, "Ultra-wideband capacity enhancement of 50  $\mu\text{m}$  multimode fiber links up to 3 km using orthogonal polarization transmission in C-band," in *Proc. Eur. Conf. Opt. Commun.*, Copenhagen, Denmark, Sep. 8–12, 2002, vol. 2, p. 2.
- [14] S. Fan and J. M. Kahn, "Principal modes in multimode waveguides," *Opt. Lett.*, vol. 30, no. 2, pp. 135–137, Jan. 2005.
- [15] R. Khosravani, I. T. Lima, P. Ebrahimi, E. Ibragimov, A. E. Willner, and C. R. Menyuk, "Time and frequency domain characteristics of polarization-mode dispersion emulators," *IEEE Photon. Technol. Letters*, vol. 13, no. 2, pp. 127–129, Feb. 2001.
- [16] D. Marcuse, *Theory of Dielectric Optical Waveguides*. New York: Academic, 1974, ch. 3.
- [17] D. Marcuse, *Light Transmission Optics*. New York: Bell Telephone Laboratories, 1972.
- [18] G. Ghosh and H. Yajima, "Pressure-dependent Sellmeier coefficients and material dispersions for silica fiber glass," *J. Lightw. Technol.*, vol. 16, no. 11, pp. 2002–2005, Nov. 1998.
- [19] S. C. Rashleigh, "Origins and control of polarization effects in single-mode fibers," *J. Lightw. Technol.*, vol. LT-1, no. 2, pp. 312–331, Jun. 1983.
- [20] K. Iizuka, *Elements of Photonics in Free Space and Special Media*. New York: Wiley, 2002, p. 383.
- [21] B. K. Garside, T. K. Lim, T. K. , and J. P. Marton, "Propagation characteristics of parabolic-index fiber modes: Linearly polarized approximation," *J. Opt. Soc. Amer.*, vol. 70, no. 4, pp. 395–400, Apr. 1980.
- [22] C. Cohen-Tannoudji, B. Diu, and F. Laloë, *Quantum Mechanics*. New York: Wiley, 1977.
- [23] A. W. Snyder and J. D. Love, *Optical Waveguide Theory*. New York: Chapman & Hall Ltd., 1983, p. 309.
- [24] W. Mao, "Multimode fiber communication using adaptive spatial filtering," Ph.D. dissertation, Univ. California, Berkeley, Dec. 2005.
- [25] H. F. Taylor, "Power loss at directional change in dielectric waveguides," *Appl. Opt.*, vol. 13, no. 3, pp. 642–647, Mar. 1974.
- [26] H. F. Taylor, "Bending effects in optical fiber," *J. Lightw. Technol.*, vol. LT-2, no. 5, pp. 617–628, Oct. 1984.
- [27] H. E. Rowe, *Electromagnetic Propagation in Multi-Mode Random Media*. New York: Wiley, 1999.
- [28] A. B. Carlson, P. B. Crilly, and J. C. Rutledge, *Communication Systems*, 4th ed. New York: McGraw-Hill, 2002, p. 359, 443.
- [29] C. L. Vazquez, *Multiple Precession Toolbox for Matlab* The Digital Map Inc. [Online]. Available: <http://www.thedigitalmap.com/~carlos/software/>, 2007
- [30] D. Goldstein, *Polarized Light*, 2nd ed. New York: Marcel Dekker, 2003, pp. 21–47.
- [31] S. Betti, F. Curti, B. Daino, G. De Marchis, E. Iannone, and F. Matera, "Evolution of the bandwidth of the principal states of polarization in single-mode fibers," *Opt. Lett.*, vol. 16, no. 7, pp. 467–469, Apr. 1991.



**Mahdieh B. Shemirani** received the B.Sc. degree in electrical engineering from Sharif University of Technology, Tehran, Iran, in 2004, and the M.Sc. degree in electrical engineering from Stanford University, Stanford, CA, in 2006, where she is currently working toward the Ph.D. degree in electrical engineering.

Her current interests include fiber modeling, performance optimization of optical communication systems using adaptive optics, and utilizing Fourier optics techniques in designing analog Fourier trans-

form processors in RF domain.

Ms. Shemirani is the recipient of Stanford Graduate Fellowship in 2004–2007.

**Wei Mao** received the B.A. degree in physics, and the M.S. and Ph.D. degrees in electrical engineering from the University of California at Berkeley in 1998, 2001, and 2005, respectively.

She is currently working as a Senior Research Engineer at Robert Bosch LLC, Palo Alto, CA. Her current research interests include various topics in MIMO wireless communications.

**Rahul Alex Panicker** received the B.Tech. degree from the Indian Institute of Technology (IIT), Madras, India, in 2002, an M.S. and Ph.D. degrees from Stanford University, Stanford, CA, in 2004 and 2007 respectively, all in electrical engineering.

He is currently working as a Chief Technology Officer at Embrace, Stanford, CA. His research interests include applying convex-optimization techniques to optical communications systems and designing next-generation systems based on Infinera's photonic-integrated-circuit technology. He also spends time at the Stanford Institute of Design, where he does design for the developing world.



**Joseph M. Kahn** (M'90–SM'98–F'00) received the A.B., M.A., and Ph.D. degrees in physics from the University of California at Berkeley in 1981, 1983 and 1986, respectively.

From 1987 to 1990, he was with AT&T Bell Laboratories, Crawford Hill Laboratory, Holmdel, NJ. He demonstrated multi-Gb/s coherent optical fiber transmission systems, setting world records for receiver sensitivity. From 1990 to 2003, he was on the faculty of the Department of Electrical Engineering and Computer Sciences at UC Berkeley, performing research on optical and wireless communications. Since 2003, he has been a Professor of Electrical Engineering at Stanford University. His current research interests include single- and multi-mode optical fiber communications, free-space optical communications, and MEMS for optical communications. In 2000, he helped found StrataLight Communications, where he served as Chief Scientist from 2000 to 2003.

Prof. Kahn received the National Science Foundation Presidential Young Investigator Award in 1991. From 1993 to 2000, he served as a Technical Editor of *IEEE Personal Communications Magazine*.